J. Phys. B: At. Mol. Opt. Phys. **32** (1999) 5523–5538. Printed in the UK PII: S0953-4075(99)04960-3

Elastic and rotationally inelastic cross sections for low-energy electron scattering by SO_2 molecules

A P P Natalense†§, M T do N Varella†‖, M H F Bettega‡, L G Ferreira† and M A P Lima†

† Instituto de Física Gleb Wataghin, Universidade Estadual de Campinas, Unicamp, 13083-970 Campinas, São Paulo, Brazil

‡ Departamento de Física, Universidade Federal do Paraná, Caixa Postal 19081, 81531-990, Curitiba, Paraná, Brazil

Received 7 June 1999, in final form 17 September 1999

Abstract. We show rotationally summed and rotationally inelastic differential, integral and momentum transfer cross sections for electron scattering by SO_2 in the 3–30 eV impact energy range in the static exchange approximation. Our results were obtained with the Schwinger multichannel method with pseudopotentials, including a first Born approximation to describe the influence of the molecular permanent dipole moment on the scattering cross sections. The rotational excitation cross sections were obtained through the adiabatic-nuclei-rotation approximation. Our results show good agreement with available experimental and theoretical data. The rotationally inelastic cross sections were found to be very large.

1. Introduction

Among the atmospheric pollutants, SO_2 is one of highest environmental concern [1]. It is also present in the atmosphere of Jupiter and its satellite Io, where the interactions of SO_2 with electrons play an important role in the magnetosphere plasma dynamics [2].

For the electron-impact energies we study here there is a wide variety of experimental results on electron interactions with SO_2 molecules, such as electron-impact dissociation [3], ionization [4], vibrational excitation [5], total cross sections [6], and elastic scattering [7, 8]. However, theoretical data are scarce. A theoretical study on electron-impact total ionization cross sections was recently published [9], but, to our knowledge, there are only two published studies concerning the electron scattering process we address in this paper: the first one shows results for momentum transfer cross sections (MTCS) [10] (along with electronic excitation and ionization cross sections), and the second [11] presents elastic scattering and rotational excitation cross sections. We have also digitized the complex Kohn results [12] shown in [7] as a private communication. In this paper we show elastic (rotationally summed) and rotationally resolved differential cross sections (DCS), integral cross sections (ICS) and MTCS for electron scattering from SO_2 in the 3–30 eV impact energy range, in the static exchange approximation.

Our elastic cross sections were calculated using the Schwinger multichannel (SMC) method [13] implemented with pseudopotentials [14] (SMCPP). The nuclei and the core

§ Present address: Department of Chemistry, Texas A&M University, College Station, TX 77843-3255, USA.

‖ Present address: A A Noyes Laboratory of Chemical Physics, California Institute of Technology, Pasadena, CA 91125, USA.

0953-4075/99/235523+16$30.00

electrons of each atom (in the present study 1s for oxygen and 1s, 2s and 2p for sulfur) are replaced by the norm-conserving pseudopotentials of [15] and the molecular valence is described within the Hartree–Fock (HF) framework. We have been using this method to study the electron scattering by several different molecules at different levels of approximation. Our most recent applications are elastic scattering by H_2O, H_2S, H_2Se, H_2Te, CHF_3, CH_2F_2, CH_3F, $CHCl_3$, CH_2Cl_2, CH_3Cl, $CFCl_3$, CF_2Cl_2, CF_3Cl, $As(CH_3)_3$ (TMAs), O_3, N_2, P_2, As_2, Sb_2, B_2H_6, C_2H_6, Si_2H_6 and Ge_2H_6 [16]; electronic excitation by electron impact of XH_4 (X = C, Si, Ge, Sn, Pb), and H_2 [17]; elastic scattering and rotational excitations of CF_4, CCl_4, $SiCl_4$, $SiBr_4$ and Si_4 [18]; rotational excitations of YH_3 (Y = N, P, As, Sb) [19], and XH_4 (X = C, Si, Ge, Sn, Pb) [20]; and electronic excitations by electron impact including polarization effects of Na_2 [21].

The rotational excitation cross sections were calculated through the well known adiabatic-nuclei-rotation (ANR) approximation [22]. This approximation was first adapted to electron–molecule scattering problems in 1967 [23] in an application to the scattering of electrons from H_2^+. Gianturco *et al* introduced symmetry adapted functions to the method, which allowed the study of polyatomic targets [24].

The SO_2 molecule presents a typical separation between neighbouring rotational levels around 10^{-4} eV, and a relatively large dipole moment (1.63 D [25]). As a consequence, one should expect large rotationally inelastic cross sections, which have indeed been observed by Gianturco *et al* [11].

The SMC method is a $\mathcal{L}^2$ method which only requires a good description of the wavefunction within the range of the potential. This characteristic of the method has important implications when long-range potentials (such as the dipole potential) are involved. In this case, square-integrable functions may vanish in the spatial region where the potential still has significant values. In fact, the somewhat large molecular permanent dipole moment produces long-range interactions which are expected to be relevant in e^-–SO_2 collisions. To include the effect of the dipole potential in our calculations we use the first Born approximation (FBA) to compute the scattering of an electron by a rotating dipole. There are several applications of the FBA to scattering processes in the literature [26]. Recent applications include, for example, calculations of the first rotational excitation cross sections for H_2O and NH_3 [27], high partial-wave corrections for electron scattering from non-polar molecules [28], and corrections to account for the effect of the permanent dipole moment of CO on the positron-scattering process [29]. Our detailed procedure is given elsewhere [19]. The basic idea is to rotationally resolve the elastic cross section and to work with the scattering amplitude for the dipole-allowed ($J = 0 \rightarrow J' = 1$) rotational excitation. The low partial waves (up to some $l = l_1$) of the ($J = 0 \rightarrow J' = 1$) scattering amplitude, are described through the SMCPP, while the high partial waves ($l_1 < l < \infty$) are described through the FBA of the dipole potential. The values of l_1 are, in general, different for each impact energy and are chosen in such a way that the ($J = 0 \rightarrow J' = 1$) DCS obtained with SMCPP plus Born closure shows the smallest deviation from the pure SMCPP DCS for high scattering angles. To avoid the divergence of the ($J = 0 \rightarrow J' = 1$) DCS at the incident direction, we take advantage of the rotational energy transfer to make $|\vec{k}_{\rm in}| \neq |\vec{k}_{\rm out}|$. This procedure enables us to obtain rotationally summed ICS.

This paper is organized as follows: the theoretical formulation of both elastic and rotationally inelastic scattering is given in section 2, while computational procedures are detailed in section 3. Our results are shown and discussed in section 4, and the conclusions are presented in section 5. Tables 1–6 show our cross sections, for ready comparison with future works. Our rotationally resolved DCSs are shown at selected energies.

Table 1. Cartesian Gaussian function exponents.

	Sulfur	Oxygen
Type	Exponent	Exponent
s	7.649 093	16.058 78
	1.743 283	5.920 242
	0.789 128	1.034 907
	0.302 805	0.316 843
	0.063 479	0.065 203
p	7.203 417	10.141 27
	3.134 723	2.783 023
	0.529 380	0.841 010
	0.154 155	0.232 940
	0.035 523	0.052 211
d	1.689 035	1.656 468
	0.476 317	0.444 747
	0.151 558	0.144 706

2. Theoretical formulation

The SMC method is described elsewhere [13], and here we only show a brief description of its main features. In this method, the scattering wavefunction is expanded in $(N+1)$-particle Slater determinants. The coefficients of this expansion are found through the variational stability of the scattering amplitude. The final expression for the scattering amplitude in the molecular body frame is then given by

$$[f_{\vec{k}_f,\vec{k}_i}] = -\frac{1}{2\pi}\sum_{m,n}\langle S_{\vec{k}_f}|V|\chi_m\rangle(d^{-1})_{mn}\langle\chi_n|V|S_{\vec{k}_i}\rangle, \tag{1}$$

where

$$d_{mn} = \langle\chi_m|A^{(+)}|\chi_n\rangle, \tag{2}$$

and

$$A^{(+)} = \frac{\hat{H}}{N+1} - \frac{(\hat{H}P + P\hat{H})}{2} + \frac{(VP + PV)}{2} - VG_P^{(+)}V. \tag{3}$$

In the expressions above, $S_{\vec{k}_{i,f}}$ are solutions of the unperturbed Hamiltonian (molecular Hamiltonian plus the kinetic energy operator for the incident electron). V is the interaction potential between the incident electron and the molecular target; $|\chi_n\rangle$ is a $(N+1)$-particle Slater determinant; $\hat{H}$ is the total energy minus the full Hamiltonian of the problem; P is a projector operator onto the open channel space, which is defined by energetically accessible target states; and $G_P^{(+)}$ is the free-particle Green function projected onto the space defined by P. All matrix elements but those of $\langle\chi_m|VG_P^{(+)}V|\chi_n\rangle$, which we call VGV matrix elements, can be calculated analytically. The numerical evaluation of VGV matrix elements [30] is the most time-consuming step of the SMC code, and is drastically reduced with the use of pseudopotentials.

In order to obtain rotational excitation cross sections, the elastic scattering amplitudes, originally calculated in the body-fixed frame (BF) of the molecular target, are transformed into the laboratory-fixed frame (LF) through the relation

$$f^{\text{lab}}(k_{\text{in}}, \vec{k}'_{\text{out}}, \Omega) = \sum_{\ell\mu} Y_{\ell\mu}(\hat{k}'_{\text{out}})\, f^{\text{lab}}_{\ell\mu}(\alpha, \beta, \gamma), \tag{4}$$

Table 2. Differential elastic cross sections for SO_2 (10^{-16} cm^2).

Angle (deg)	3.4 eV	5 eV	10 eV	12 eV	15 eV	20 eV	30 eV
5	115.482	81.682	47.707	43.572	41.997	36.056	29.476
10	31.262	24.276	18.591	18.990	21.731	20.429	18.204
15	15.522	13.337	12.481	13.433	16.361	15.773	13.908
20	9.857	9.183	9.614	10.486	12.892	12.454	10.452
25	7.092	6.958	7.640	8.255	9.963	9.516	7.442
30	5.463	5.491	6.054	6.386	7.408	6.933	4.998
35	4.379	4.400	4.730	4.818	5.268	4.786	3.192
40	3.596	3.539	3.637	3.551	3.588	3.126	1.988
45	3.001	2.843	2.766	2.581	2.367	1.950	1.263
50	2.534	2.276	2.098	1.879	1.550	1.194	0.866
55	2.157	1.820	1.611	1.402	1.057	0.767	0.663
60	1.849	1.454	1.271	1.098	0.792	0.569	0.559
65	1.592	1.167	1.047	0.916	0.671	0.511	0.501
70	1.376	0.946	0.909	0.817	0.630	0.522	0.466
75	1.191	0.781	0.835	0.770	0.626	0.553	0.443
80	1.034	0.666	0.807	0.757	0.639	0.578	0.430
85	0.903	0.596	0.812	0.767	0.660	0.586	0.423
90	0.798	0.568	0.843	0.795	0.688	0.581	0.418
95	0.720	0.579	0.891	0.837	0.725	0.569	0.414
100	0.674	0.627	0.950	0.889	0.770	0.561	0.410
105	0.659	0.709	1.014	0.947	0.821	0.565	0.408
110	0.679	0.821	1.077	1.006	0.875	0.582	0.410
115	0.733	0.957	1.136	1.062	0.925	0.611	0.416
120	0.820	1.113	1.186	1.111	0.969	0.644	0.424
125	0.937	1.281	1.228	1.152	1.005	0.674	0.430
130	1.078	1.457	1.265	1.186	1.035	0.696	0.433
135	1.239	1.635	1.299	1.218	1.062	0.709	0.431
140	1.413	1.813	1.337	1.253	1.092	0.716	0.427
145	1.593	1.986	1.383	1.296	1.134	0.725	0.425
150	1.771	2.152	1.440	1.352	1.190	0.743	0.433
155	1.940	2.306	1.507	1.420	1.262	0.775	0.456
160	2.092	2.444	1.580	1.498	1.344	0.819	0.495
165	2.220	2.561	1.652	1.576	1.428	0.871	0.544
170	2.317	2.650	1.714	1.643	1.502	0.920	0.593
175	2.378	2.706	1.755	1.688	1.551	0.955	0.629
180	2.399	2.725	1.770	1.705	1.569	0.968	0.643

where

$$f^{\text{lab}}_{\ell\mu}(\alpha, \beta, \gamma) = \sum_{m} D^{\ell}_{\mu m}(-\gamma, -\beta, -\alpha) f^{B}_{\ell m}(\beta, \alpha). \tag{5}$$

In the expressions above, f^{lab} denotes the elastic scattering amplitude in the LF, $D^{\ell}_{\mu m}$ are Wigner rotation matrices [31] and $f^{B}_{\ell m}$ are the coefficients of the expansion of the BF scattering amplitude in spherical harmonics. It should also be noted that $\hat{k}'_{\text{out}}$ is the scattering direction in the LF, while $\vec{k}_{\text{in}} = (k_{\text{in}}, \theta_{\text{in}}, \phi_{\text{in}})$ and $\vec{k}_{\text{out}} = (k_{\text{out}}, \theta_{\text{out}}, \phi_{\text{out}})$ are, respectively, the wavevectors of the incident and outgoing particle in the BF. $\Omega = (\alpha, \beta, \gamma)$ denotes the Euler angles of the frame transformation. The Oz axis in the LF is defined along the incident direction $\hat{k}_{\text{in}} = (\alpha, \beta)$ with the Euler angle γ being arbitrary.

Table 3. ICS and MTCS for SO_2 (10^{-16} cm^2).

Energy (eV)	ICS	MTCS
3.0	35.48	15.88
3.4	33.94	16.24
4.0	32.30	16.80
4.5	31.32	17.19
5.0	30.61	17.53
5.5	30.17	17.87
6.0	29.99	18.18
6.5	29.96	18.39
7.0	29.90	18.39
7.5	29.73	18.19
8.0	29.47	17.89
8.5	29.17	17.57
9.0	28.88	17.26
9.5	28.62	16.99
10.0	28.40	16.76
11.0	28.08	16.41
12.0	28.04	16.25
13.0	28.32	16.11
14.0	28.59	15.77
15.0	28.59	15.23
16.0	28.21	14.52
17.0	27.50	13.77
18.0	26.64	13.08
19.0	25.76	12.48
20.0	24.81	11.85
21.0	24.05	11.45
23.0	22.79	10.83
25.0	21.80	10.34
26.0	21.36	10.12
29.0	20.18	9.45
30.0	19.83	9.21

The ANR approximation expression for the rotational excitation scattering amplitude is given by [22]

$$f(J\tau K \to J'\tau' K'; k_{\rm in}, \vec{k}'_{\rm out}) = \langle \Psi^s_{J'\tau' M'}(\Omega) | f^{\rm lab}(k_{\rm in}, \vec{k}'_{\rm out}, \Omega) | \Psi^s_{J\tau M}(\Omega) \rangle. \tag{6}$$

The symmetry-adapted rotational eigenfunctions of an asymmetric top, $\Psi^s_{J\tau M}(\Omega)$, are written as

$$\Psi^s_{J\tau M}(\Omega) = \sum_{K=0}^{J} \sum_{\nu=0}^{1} a^{J\tau}_{KM} \Phi^s_{JKM}(\Omega), \tag{7}$$

where

$$\Phi^s_{JKM}(\Omega) = \frac{1}{\sqrt{2}} [\Psi_{JKM} + (-1)^\nu \Psi_{J-KM}]; \qquad K > 0, \quad \nu = 0, 1, \tag{8}$$

$$\Phi^s_{JKM}(\Omega) = \Psi_{JKM}; \qquad K = 0. \tag{9}$$

It is to be observed that Ψ_{JKM} are rotational eigenfunctions of a symmetric top. J is the molecular angular momentum; K and M are, respectively, its projections onto the quantization axis of the BF and LF frames; and τ is a pseudoquantum number used to label

Table 4. $J \rightarrow J'$ rotationally resolved DCS (10^{-16} cm^2) for SO_2 at 5 and 10 eV. (For each J', we summed over τ'.)

Angle	5 eV					10 eV				
(deg)	$0 \rightarrow 0$	$0 \rightarrow 1$	$0 \rightarrow 2$	$0 \rightarrow 3$	$0 \rightarrow 4$	$0 \rightarrow 0$	$0 \rightarrow 1$	$0 \rightarrow 2$	$0 \rightarrow 3$	$0 \rightarrow 4$
0	5.352	—	1.062	0.000	0.277	10.46	—	0.145	0.000	0.254
5	5.276	75.08	1.053	0.002	0.276	10.26	37.05	0.143	0.003	0.253
10	5.053	17.92	1.027	0.008	0.272	9.694	8.496	0.137	0.012	0.250
15	4.702	7.365	0.987	0.018	0.265	8.812	3.262	0.132	0.027	0.246
20	4.250	3.708	0.938	0.031	0.256	7.701	1.489	0.134	0.046	0.240
25	3.730	2.053	0.883	0.046	0.245	6.460	0.726	0.147	0.068	0.233
30	3.177	1.190	0.828	0.062	0.232	5.191	0.362	0.173	0.093	0.225
35	2.625	0.703	0.774	0.078	0.218	3.984	0.187	0.211	0.118	0.216
40	2.101	0.416	0.722	0.095	0.203	2.907	0.108	0.254	0.143	0.207
45	1.628	0.244	0.669	0.111	0.187	2.005	0.080	0.295	0.167	0.198
50	1.218	0.141	0.615	0.126	0.173	1.294	0.076	0.326	0.188	0.189
55	0.878	0.081	0.557	0.140	0.159	0.773	0.082	0.339	0.206	0.181
60	0.607	0.048	0.495	0.152	0.147	0.419	0.090	0.335	0.221	0.174
65	0.401	0.030	0.430	0.163	0.136	0.204	0.094	0.314	0.231	0.167
70	0.251	0.023	0.363	0.173	0.128	0.092	0.092	0.285	0.238	0.161
75	0.149	0.022	0.299	0.182	0.122	0.052	0.084	0.256	0.241	0.156
80	0.085	0.024	0.241	0.189	0.117	0.054	0.073	0.237	0.240	0.152
85	0.051	0.029	0.196	0.195	0.114	0.077	0.058	0.238	0.235	0.147
90	0.039	0.036	0.166	0.199	0.113	0.104	0.043	0.263	0.227	0.142
95	0.044	0.046	0.156	0.202	0.114	0.126	0.028	0.313	0.215	0.137
100	0.060	0.060	0.168	0.202	0.116	0.136	0.017	0.384	0.199	0.132
105	0.082	0.078	0.203	0.199	0.119	0.135	0.009	0.469	0.180	0.128
110	0.108	0.101	0.258	0.194	0.124	0.123	0.005	0.560	0.158	0.125
115	0.136	0.129	0.331	0.187	0.130	0.105	0.005	0.647	0.135	0.123
120	0.163	0.163	0.417	0.177	0.137	0.083	0.008	0.722	0.111	0.124
125	0.188	0.202	0.512	0.166	0.145	0.061	0.013	0.781	0.090	0.128
130	0.211	0.245	0.610	0.154	0.154	0.042	0.019	0.820	0.074	0.136
135	0.233	0.291	0.708	0.142	0.163	0.027	0.025	0.841	0.066	0.148
140	0.253	0.339	0.802	0.131	0.172	0.016	0.030	0.847	0.067	0.164
145	0.271	0.388	0.891	0.122	0.182	0.010	0.033	0.846	0.079	0.183
150	0.288	0.435	0.974	0.115	0.190	0.007	0.034	0.841	0.102	0.205
155	0.305	0.479	1.049	0.110	0.198	0.007	0.034	0.837	0.132	0.228
160	0.319	0.518	1.115	0.107	0.206	0.008	0.032	0.838	0.167	0.251
165	0.332	0.551	1.170	0.106	0.212	0.010	0.030	0.842	0.202	0.272
170	0.341	0.575	1.212	0.106	0.216	0.012	0.028	0.848	0.232	0.288
175	0.347	0.589	1.238	0.107	0.219	0.014	0.026	0.854	0.252	0.299
180	0.349	0.594	1.247	0.107	0.220	0.014	0.026	0.856	0.259	0.303

the asymmetric top eigenfunctions and eigenvalues. One needs this pseudoquantum number because K is not a good quantum number for an asymmetric top. The procedure to obtain $\Psi^s_{J\tau M}(\Omega)$ eigenfunctions, i.e. to calculate the expansion coefficients $a^{J\tau}_{KM}$, is detailed in [32,33]. The rotational excitation cross sections are therefore given by

$$\frac{\mathrm{d}\sigma}{\mathrm{d}\Omega}(J\tau \rightarrow J'\tau';\theta'_{\mathrm{out}}) = \frac{1}{2\pi}\frac{1}{(2J+1)}\sum_{M=-J}^{J}\sum_{M'=-J'}^{J'}\frac{k_{J'\tau'}}{k_{J\tau}}\int_0^{2\pi}\mathrm{d}\phi\,|f_{J\tau M\rightarrow J'\tau'M'}|^2. \tag{10}$$

In order to take long-range interactions into account, we use the same approach as [19]. Since one is dealing with excitations departing from the rotational ground state, $|J=0;\tau=0\rangle$,

Table 5. $J \rightarrow J'$ rotationally resolved DCS (10^{-16} cm^2) for SO_2 at 20 and 30 eV. (For each J', we summed over τ'.)

Angle	20 eV					30 eV				
(deg)	$0 \rightarrow 0$	$0 \rightarrow 1$	$0 \rightarrow 2$	$0 \rightarrow 3$	$0 \rightarrow 4$	$0 \rightarrow 0$	$0 \rightarrow 1$	$0 \rightarrow 2$	$0 \rightarrow 3$	$0 \rightarrow 4$
0	18.09	—	0.778	0.000	0.153	17.79	—	0.691	0.000	0.072
5	17.58	17.56	0.760	0.004	0.151	17.11	11.61	0.675	0.011	0.072
10	16.11	3.447	0.710	0.017	0.144	15.23	2.224	0.635	0.042	0.070
15	13.90	1.059	0.644	0.035	0.133	12.49	0.668	0.588	0.088	0.068
20	11.27	0.428	0.576	0.057	0.119	9.403	0.281	0.554	0.139	0.066
25	8.524	0.281	0.520	0.079	0.105	6.430	0.206	0.541	0.187	0.064
30	5.974	0.278	0.481	0.099	0.092	3.934	0.212	0.546	0.224	0.065
35	3.827	0.293	0.454	0.118	0.081	2.093	0.216	0.550	0.246	0.069
40	2.192	0.280	0.429	0.135	0.075	0.916	0.191	0.534	0.250	0.075
45	1.079	0.232	0.394	0.150	0.074	0.291	0.141	0.485	0.240	0.084
50	0.419	0.164	0.344	0.163	0.079	0.045	0.082	0.403	0.217	0.093
55	0.102	0.093	0.279	0.175	0.088	0.010	0.033	0.301	0.187	0.101
60	0.006	0.038	0.209	0.182	0.099	0.057	0.006	0.199	0.155	0.106
65	0.023	0.008	0.144	0.184	0.110	0.107	0.005	0.116	0.125	0.107
70	0.076	0.004	0.097	0.178	0.118	0.127	0.025	0.064	0.099	0.103
75	0.117	0.019	0.074	0.165	0.122	0.116	0.057	0.043	0.077	0.096
80	0.131	0.043	0.076	0.145	0.120	0.085	0.089	0.047	0.061	0.089
85	0.118	0.067	0.097	0.121	0.113	0.051	0.113	0.064	0.050	0.082
90	0.088	0.084	0.131	0.096	0.104	0.024	0.125	0.082	0.043	0.079
95	0.055	0.092	0.169	0.075	0.094	7.5E−3	0.125	0.096	0.042	0.079
100	0.028	0.092	0.207	0.060	0.086	1.0E−3	0.116	0.104	0.045	0.084
105	0.010	0.087	0.240	0.051	0.084	1.5E−4	0.102	0.107	0.051	0.094
110	1.1E−3	0.081	0.267	0.049	0.087	1.1E−3	0.086	0.109	0.057	0.109
115	6.4E−4	0.076	0.285	0.050	0.098	1.9E−3	0.071	0.111	0.063	0.128
120	3.3E−3	0.073	0.292	0.053	0.115	1.8E−3	0.056	0.115	0.066	0.150
125	6.7E−3	0.074	0.287	0.054	0.136	1.4E−3	0.043	0.119	0.065	0.173
130	8.8E−3	0.076	0.270	0.053	0.160	1.2E−3	0.031	0.122	0.060	0.195
135	8.8E−3	0.080	0.245	0.048	0.185	8.6E−4	0.022	0.122	0.053	0.213
140	7.1E−3	0.083	0.215	0.040	0.208	5.3E−4	0.014	0.118	0.046	0.228
145	4.8E−3	0.085	0.189	0.033	0.230	2.1E−4	0.010	0.113	0.041	0.239
150	2.8E−3	0.084	0.171	0.027	0.249	4.0E−4	7.5E−3	0.108	0.041	0.249
155	2.1E−3	0.081	0.166	0.024	0.267	1.8E−3	7.4E−3	0.106	0.047	0.260
160	3.1E−3	0.076	0.174	0.025	0.282	5.0E−3	8.3E−3	0.108	0.058	0.273
165	5.3E−3	0.069	0.191	0.028	0.295	0.010	0.010	0.114	0.073	0.287
170	8.1E−3	0.063	0.211	0.032	0.306	0.015	0.011	0.122	0.086	0.299
175	0.010	0.058	0.227	0.036	0.312	0.019	0.011	0.129	0.096	0.308
180	0.011	0.057	0.233	0.037	0.315	0.020	0.012	0.132	0.100	0.312

the only dipole-allowed rotational transition will be ($J = 0, \tau = 0 \rightarrow J' = 1, \tau' = 0$), for which a Born closure procedure is applied. Combining the ANR approximation and the FBA, one can obtain an expression for the ($J = 0, \tau = 0 \rightarrow J' = 1, \tau' = 0$) rotational excitation:

$$f^{\mathrm{FBA}}(J\tau M \rightarrow J'\tau' M'; \vec{k}'_{\mathrm{out}}) = \int \mathrm{d}\Omega\, \Psi^{s*}_{J'\tau' M'}(\Omega) f^{\mathrm{DIP}}_{\mathrm{FBA}}(\beta, \gamma, \vec{k}'_{\mathrm{out}}) \Psi^{s}_{J\tau M}(\Omega), \tag{11}$$

where

$$f^{\mathrm{DIP}}_{\mathrm{FBA}}(k, \hat{k}_{\mathrm{in}}, \hat{k}_{\mathrm{out}}) = 2\mathrm{i}\frac{\vec{D} \cdot (\vec{k}_{\mathrm{in}} - \vec{k}_{\mathrm{out}})}{|\vec{k}_{\mathrm{in}} - \vec{k}_{\mathrm{out}}|^2}. \tag{12}$$

Table 6. $J \rightarrow J'$ rotationally resolved ICS and MTCS for SO_2 (10^{-16} cm^2). (For each J', we summed over τ'.)

Energy	ICS					MTCS				
(eV)	$0 \rightarrow 0$	$0 \rightarrow 1$	$0 \rightarrow 2$	$0 \rightarrow 3$	$0 \rightarrow 4$	$0 \rightarrow 0$	$0 \rightarrow 1$	$0 \rightarrow 2$	$0 \rightarrow 3$	$0 \rightarrow 4$
5.0	8.893	10.760	6.455	1.899	1.950	3.364	2.706	6.578	2.028	1.869
6.0	9.071	8.847	6.652	2.165	2.275	2.899	2.037	7.670	2.114	1.983
7.0	10.140	7.250	6.704	2.213	2.332	2.714	1.260	8.634	2.028	1.896
8.0	11.190	6.047	6.406	2.145	2.221	2.719	0.720	8.563	1.966	1.827
9.0	11.730	5.261	6.023	2.100	2.136	2.625	0.507	7.971	1.967	1.884
10.0	11.960	4.769	5.697	2.052	2.106	2.433	0.518	7.303	1.954	2.017
11.0	12.090	4.458	5.449	1.950	2.107	2.217	0.646	6.693	1.873	2.178
12.0	12.310	4.255	5.290	1.768	2.132	2.019	0.830	6.204	1.696	2.353
13.0	12.830	4.103	5.137	1.541	2.157	1.881	1.016	5.761	1.454	2.494
14.0	13.530	3.961	4.857	1.352	2.130	1.821	1.141	5.235	1.237	2.521
15.0	14.090	3.870	4.468	1.238	2.037	1.801	1.256	4.647	1.092	2.416
16.0	14.350	3.764	4.074	1.178	1.904	1.783	1.287	4.094	1.004	2.240
17.0	14.290	3.634	3.734	1.156	1.773	1.753	1.273	3.623	0.953	2.068
18.0	14.010	3.495	3.464	1.158	1.674	1.706	1.234	3.240	0.930	1.942
19.0	13.600	3.358	3.257	1.175	1.612	1.643	1.184	2.929	0.923	1.873
20.0	13.130	3.116	3.101	1.198	1.582	1.566	0.996	2.679	0.922	1.854
21.0	12.640	3.012	2.984	1.222	1.577	1.482	0.944	2.471	0.923	1.870
23.0	11.740	2.845	2.831	1.261	1.603	1.308	0.865	2.153	0.918	1.960
25.0	11.020	2.733	2.716	1.286	1.631	1.157	0.822	1.927	0.907	2.048
26.0	10.720	2.690	2.658	1.291	1.635	1.096	0.810	1.843	0.902	2.069
29.0	10.040	2.550	2.470	1.258	1.597	0.969	0.766	1.625	0.878	2.003
30.0	9.868	2.500	2.394	1.219	1.566	0.943	0.747	1.534	0.859	1.933

It is to be observed that equation (12) is the FBA elastic amplitude for the dipole moment potential [34] and not for the full interaction potential. The FBA rotational scattering amplitude, given by equation (11), is analytic and provides fair results in the high partial-wave limit ($l \rightarrow \infty$). It is not a good approximation, however, to describe short-range interactions. One can overcome this difficulty by substituting the FBA low partial waves by SMCPP ones:

$$f^{\text{lab}}(J\tau M \rightarrow J'\tau' M'; \vec{k}'_{\text{out}}) = f^{\text{FBA}}(J\tau M \rightarrow J'\tau' M'; \vec{k}'_{\text{out}}) + \sum_{\substack{l=0 \\ \mu}}^{l_1} [f_{l\mu}^{\text{SMCPP}}(k_{\text{in}}, k_{\text{out}}) - f_{l\mu}^{\text{FBA}}(k_{\text{in}}, k_{\text{out}})] Y_{l\mu}(\vec{k}'_{\text{out}}). \tag{13}$$

In the expression above, $f_{l\mu}^{\text{SMCPP}}$ and $f_{l\mu}^{\text{FBA}}$ are, respectively, coefficients of expansions of equations (6) and (11) in spherical harmonics. At a given impact energy, l_1 is chosen in such a way that the $(J = 0, \tau = 0 \rightarrow J' = 1, \tau' = 0)$ DCS obtained with SMCPP plus Born closure shows the smallest deviation from the pure SMCPP DCS for high scattering angles. The Born closure approach has two interesting properties: (i) it provides better cross sections at small scattering angles for the $(J = 0, \tau = 0 \rightarrow J' = 1, \tau' = 0)$ rotational excitation; (ii) it provides a way to avoid the divergent behaviour of the $(J = 0, \tau = 0 \rightarrow J' = 1, \tau' = 0)$ rotational excitation DCS. This can be achieved by taking the rotational energy transfer into account to make $|\vec{k}_{\text{in}}| \neq |\vec{k}_{\text{out}}|$ in equation (12). These two properties can be extended to elastic differential and ICS by summing the rotationally resolved ones.

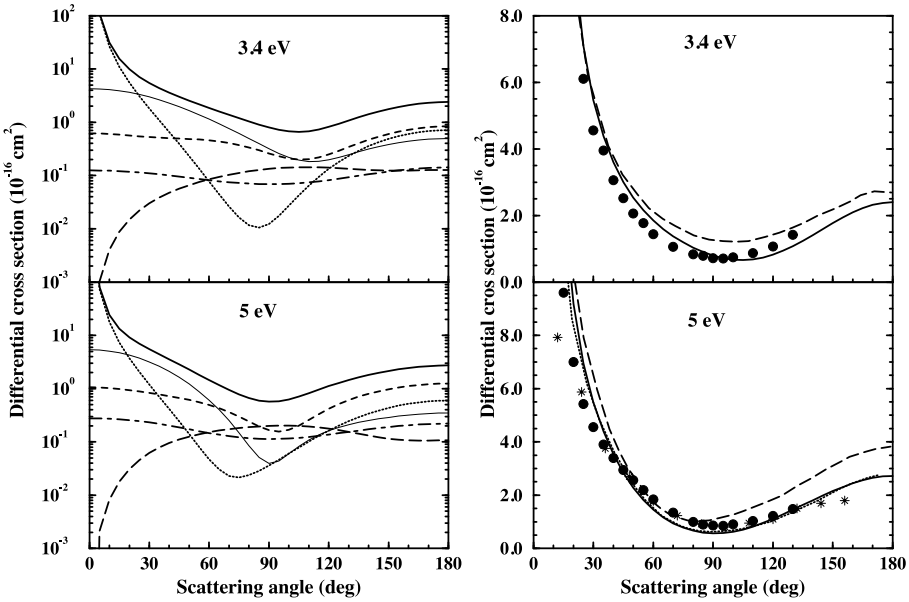

Figure 1. DCS for e^-–SO_2 scattering at 3.4 and 5 eV. Left panels: present rotationally resolved cross sections. Thick solid curve: rotationally summed DCS (SMCPP + FBA); thin solid curve: ($J = 0 \rightarrow J' = 0$) rotational excitation; dotted curve: ($J = 0 \rightarrow J' = 1$) rotational excitation (SMCPP + FBA); short-dashed curve: ($J = 0 \rightarrow J' = 2$) rotational excitation; long-dashed curve: ($J = 0 \rightarrow J' = 3$) rotational excitation; dot-dashed curve: ($J = 0 \rightarrow J' = 4$) rotational excitation. Right panels: elastic (rotationally summed) cross sections. Solid curve: present rotationally summed DCS (SMCPP + FBA); dashed curve: rotationally summed DCS of [11]; dotted curve: results using the complex Kohn method [12]; full circles: experiment [7]; stars: experiment [8].

3. Computational procedures

Our basis sets are composed of Cartesian Gaussian functions designed to be used in our pseudopotential description of the molecular target [35]. The exponents are given in table 1. It is important to note that we have not included the symmetrical components of d functions in the calculations (namely $(x^2 + y^2 + z^2)\exp(-\alpha r^2)$), in order to avoid linear dependence in the basis set [18]. Our molecular target is described within the fixed-nuclei approximation, with interatomic distance $R_{(S-O)} = 1.431$ Å and bond angle O–$\hat{S}$–O $= 119.3^\circ$ [36]. The experimental dipole moment is 1.633 D (±1%) [25] and our theoretical value, 1.92 D, is 15% higher. In the present implementation of our method, the target can only be described in a single-determinant HF framework. As a result, the theoretical dipole moment value cannot be improved, although it might be a source of error. It is to be observed, however, that we have been able to obtain differential and integral rotationally summed cross sections in good agreement with the experimental data, even though HF dipole moments are always overestimated (see Varella *et al* 1999a [16] and also [19]).

In all rotational cross section calculations performed, with the exception of the $00 \rightarrow 10$ excitation, the partial-wave decompositions of the elastic scattering amplitudes, equation (1), were truncated at $\ell = 9$, and integrations were carried out using Gauss–Legendre quadratures with 512 points (16 for $0 \leqslant \theta \leqslant \pi$ and 32 for $0 \leqslant \phi \leqslant 2\pi$). We have checked convergence of our cross sections through partial-wave analysis and found the above

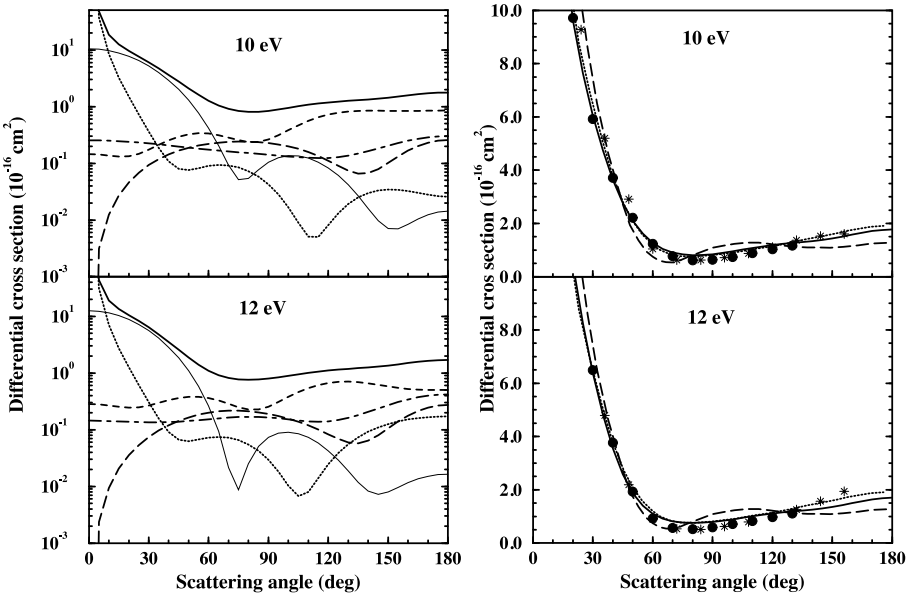

Figure 2. DCS for e^-–SO_2 scattering at 10 eV and 12 eV. Left panels: same as figure 1. Right panels: elastic (rotationally summed) cross sections. Solid curve: present rotationally summed DCS (SMCPP + FBA); dashed curve: rotationally summed DCS of [11]; dotted curve: complex Kohn results [12]; full circles: experiment [7]; stars: experiment [8].

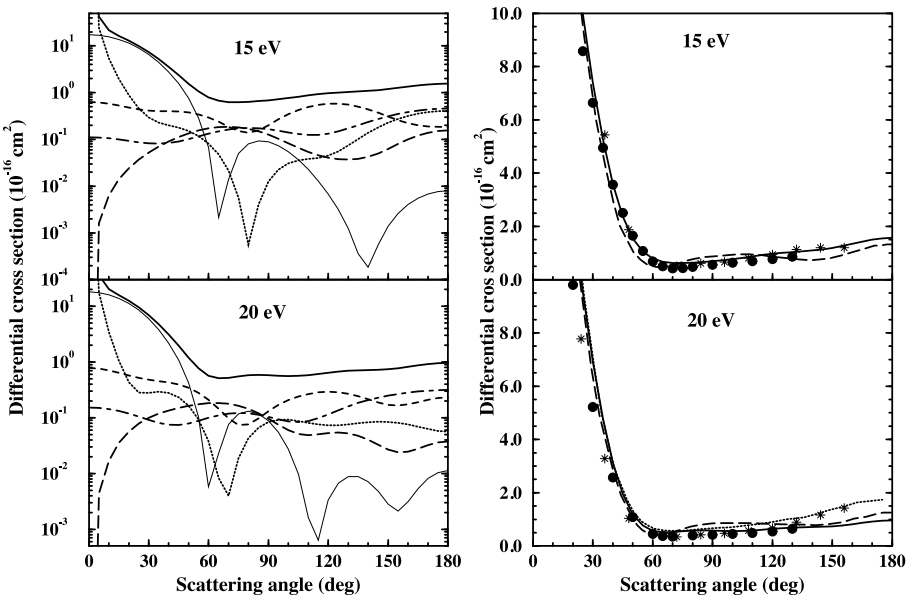

Figure 3. Same as figure 2 but for 15 and 20 eV.

quadratures and maximum angular momentum for scattering amplitude expansion to be adequate. The rotationally summed cross sections have included all excitations up to $J = 7$.

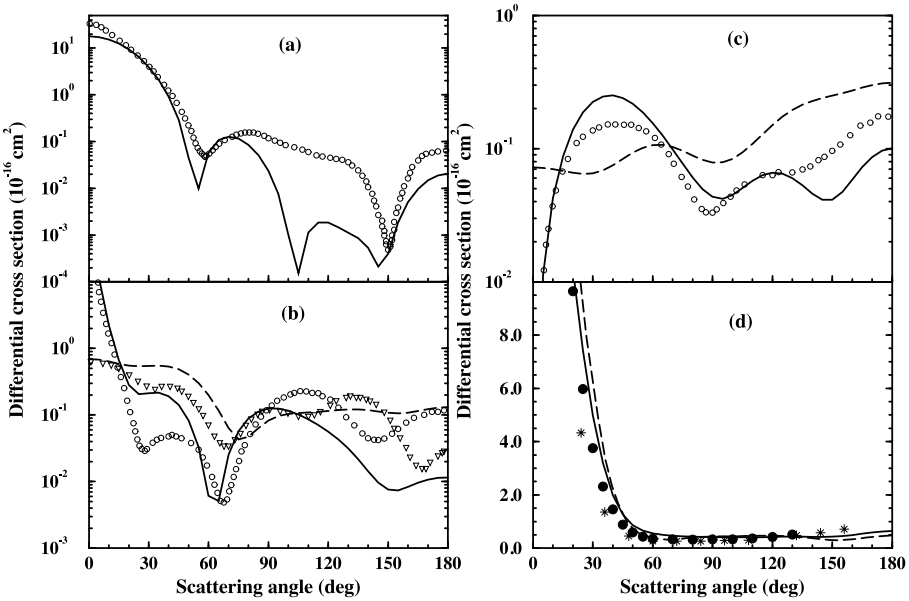

Figure 4. DCS for e^-–SO_2 scattering at 30 eV. (*a*) Rotationally resolved cross section. Solid curve: present result for $0 \rightarrow 0$ rotational excitation; open circles: calculation of [11] for $0 \rightarrow 0$ rotational excitation. (*b*) Rotationally resolved cross section. Solid curve: present result for $0 \rightarrow 1$ rotational excitation (SMCPP + FBA); open circles: calculation of [11] for $0 \rightarrow 1$ rotational excitation; dashed curve: present result for $0 \rightarrow 2$ rotational excitation; triangles: calculation of [11] for $0 \rightarrow 2$ rotational excitation. (*c*) Rotationally resolved cross section. Solid curve: present result for $0 \rightarrow 3$ rotational excitation; open circles: calculation of [11] for $0 \rightarrow 3$ rotational excitation; dashed curve: present result for $0 \rightarrow 4$ rotational excitation. (*d*) Elastic (rotationally summed) cross sections. Solid curve: present result (SMCPP + FBA); dashed curve: rotationally summed DCS of [11]; full circles: experiment [7]; stars: experiment [8].

4. Results and discussion

In figures 1–4, we show rotationally summed differential cross sections (RSDCS) and also $J = 0 \rightarrow J' = 0, 1, 2, 3, 4$ rotational excitation cross sections, summed over the pseudoquantum number τ. For comparison purposes, we have included the theoretical elastic cross sections of [11, 12] and the experimental data of [7, 8]. There is, in general, good agreement between theoretical and experimental results, even though the rotationally summed cross sections of [11] show a smooth oscillation at 10 eV and above, for angles beyond 70°. Our rotationally summed results and those of [12] do not show this oscillation and are in very good agreement with the experimental data of [7, 8]. Figures 1–4 show that the $J = 0 \rightarrow J' = 1$ rotational excitation dominates the collision process for small angles for impact energies below 15 eV, as suggested by Gianturco *et al* [11].

In figure 4 we also include the $J = 0 \rightarrow J' = 0, 1, 2, 3, 4$ rotational excitation cross sections of [11]. Apart from the fact that there are some significant discrepancies between the two sets of results for particular rotational excitations (see, for example, the $J = 0 \rightarrow J' = 0$ curves for angles between 75° and 150°), the rotationally summed cross sections produced by the two different methods are in good agreement, showing only small discrepancies at high angles.

The calculations of [11] include a description of the distortion of the molecular target due to the electric field of the incoming electron through a model correlation–polarization potential.

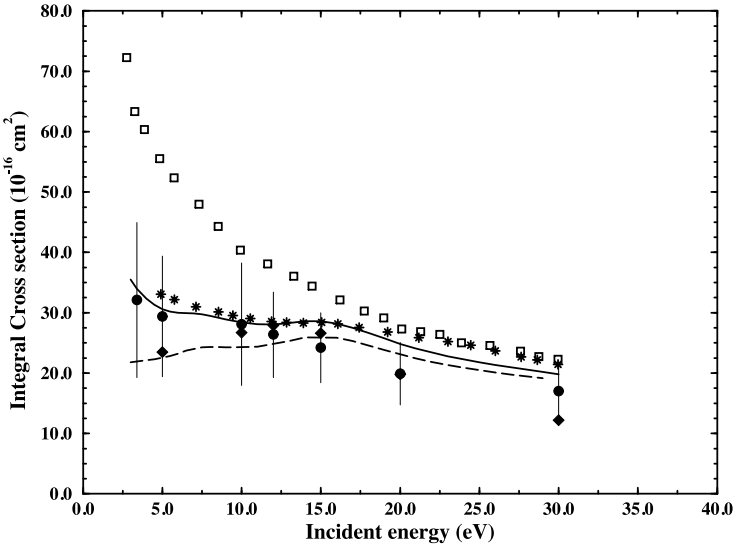

Figure 5. ICS for e^-–SO_2 scattering. Solid curve: SMCPP plus Born closure result (rotationally summed); long-dashed curve: pure SMCPP result (rotationally unresolved); stars: complex Kohn result [12]; squares: theory of [11]; full circles with error bars: experiment [7]; diamonds: experiment [8].

We have not included the description of these polarization effects in our calculations, and there are several aspects of the problem of the electron scattering from SO_2 molecules that lead us to believe that these effects could be neglected without too much degradation of our final results. Polarization effects are known to be more important for small impact energies, so that one should expect them to have little influence on the cross sections for the energy range we study here. The average polarizability of this molecule is relatively small (4.28×10^{-24} cm^3 [37]), indicating a small average response to an external field. Thus, the dipole potential produced by the somewhat large molecular dipole moment is expected to dominate the long-range electron scattering process. The agreement between our results and the experimental DCS, especially for small angles, seems to indicate that this may actually be the case.

In figure 5 we show our ICS compared with theoretical and experimental results from the literature. The solid curve shows our SMCPP plus Born closure rotationally summed results and the long-dashed curve shows our pure SMCPP elastic (rotationally unresolved) cross sections. There is a significant difference between our SMCPP and SMCPP + FBA results, pointing out that the molecular dipole potential plays a very important role in the scattering process for energies below 15 eV, as expected. Our SMCPP + FBA results agree well with the experimental points of [7] for this energy region. For energies above 15 eV, some discrepancy is found, but our cross sections do not violate the error bars of Gulley *et al* [7]. There is also good agreement between our calculations and those of [12] (dot-dashed curve). The ICS of [11] (dotted curve) seem to be overestimated, especially for energies below 15 eV.

Our MTCS, shown in figure 6, present a maximum at 5 eV, which is also seen in the measurements of Gulley *et al* [7]. The exact position of the experimental maximum is difficult to determine due to the spacing between experimental points. Our calculations also agree with complex Kohn results of [12], for energies above 10 eV, but their maximum appears at about 10 eV. The result of [10] also shows the maximum shifted by about 5 eV in energy, when compared with ours. Although the ICS of Gianturco *et al* [11] is too large, the MTCS

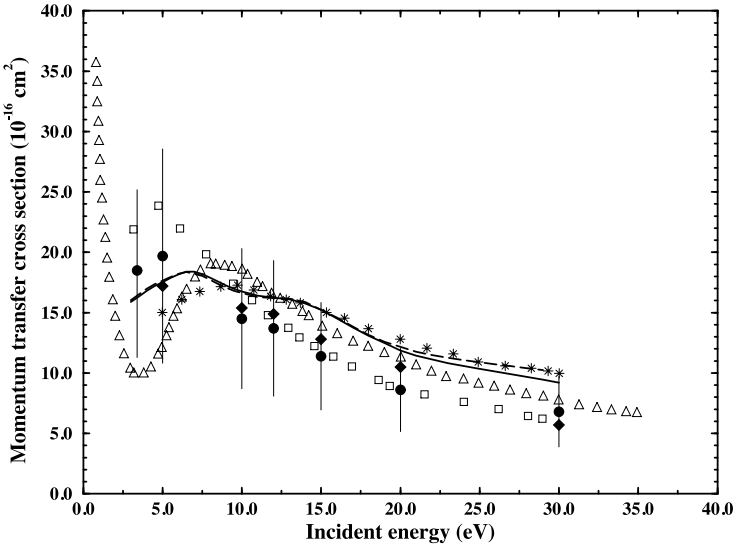

Figure 6. MTCS for e^-–SO_2 scattering. Solid curve: SMCPP plus Born closure result (rotationally summed); long-dashed curve: pure SMCPP result (rotationally unresolved); triangles: theory of [10]; stars: complex Kohn result [12]; squares: theory of [11]; full circles with error bars: experiment [7]; diamonds: experiment [8].

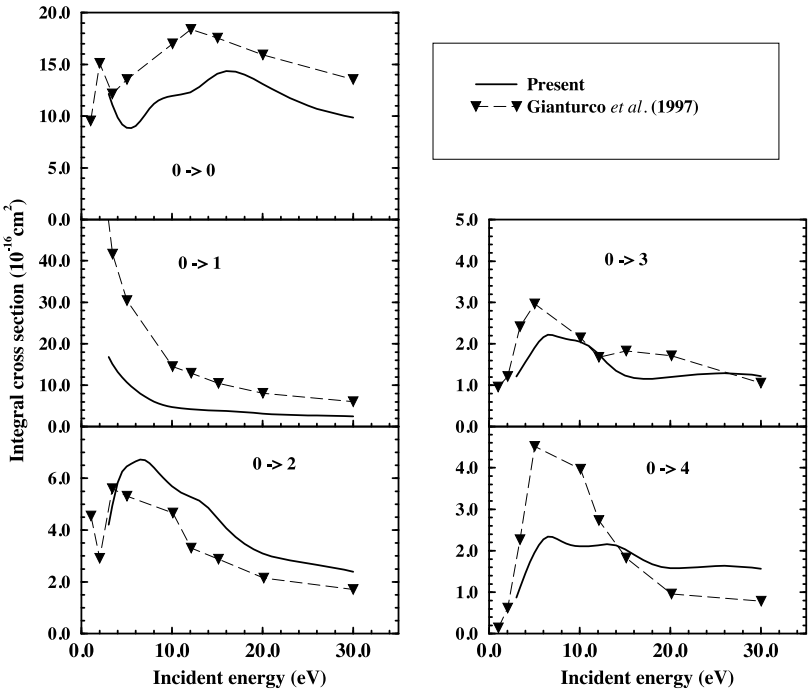

Figure 7. ICS for $J = 0 \rightarrow J' = 0, 1, 2, 3, 4$ rotational excitations. Solid curve: present results; dashed curves with triangles: theory of [11].

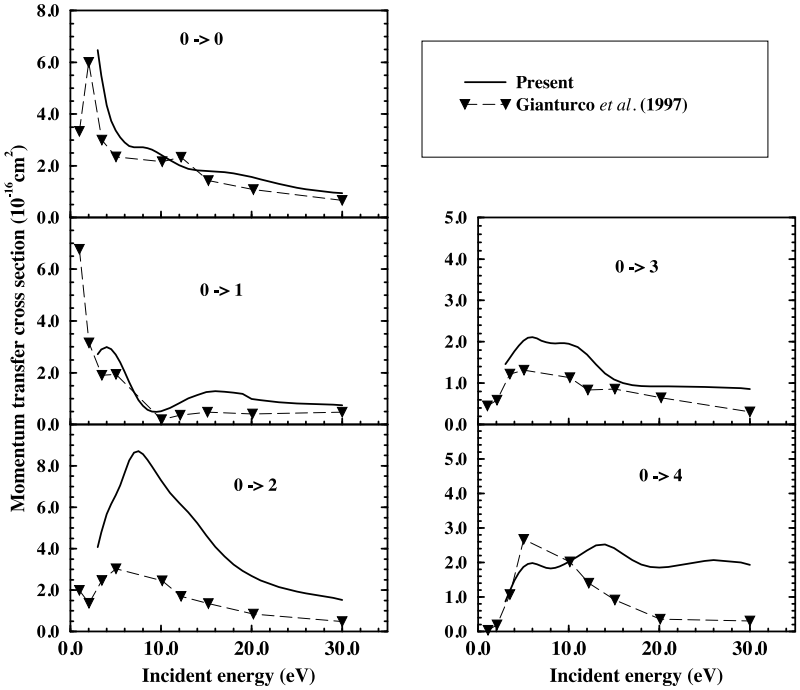

Figure 8. MTCS for $J = 0 \rightarrow J' = 0, 1, 2, 3, 4$ rotational excitations. Solid curve: present results; dashed curves with triangles: theory of [11].

show good agreement with experimental data beyond 10 eV. This fact, along with the good agreement observed in the DCS (see figures 1–4), may indicate that they are overestimating the small scattering angle contribution to the ICS. The two sets of experimental data show only a qualitative agreement with each other, but the data points of each set of results fall inside the other result's error bars. This picture clearly illustrates that the electron scattering by SO_2 molecules still has many problems to be solved, especially as far as theory is concerned.

In figures 7 and 8, we show, respectively, our rotational ICS and MTCS for $J = 0 \rightarrow J' = 0, 1, 2, 3, 4$ excitations, summed over τ, compared with the results of Gianturco *et al* [11]. There is a reasonable agreement in shape, but, quantitatively, the results are somewhat discrepant. This was to be expected since there was no good agreement in the rotationally summed cross sections of figures 5 and 6. Finally, in figure 9, we show rotationally elastic and inelastic rotationally summed ICS including $J' = 1$–7 (solid and dashed curves, respectively). The ICS for the dipole-allowed ($J = 0 \rightarrow J' = 1$) excitation (dotted curve) is also shown for comparison purposes. The rotationally summed inelastic ICS is larger than the rotationally elastic ICS for $E < 15$ eV. It is also interesting to observe that the ($J = 0 \rightarrow J' = 1$) ICS is larger than the rotationally elastic ICS for $E < 5$ eV, indicating that long-range dipole interactions dominate the low-energy scattering. For higher impact energies, however, one notices a very important contribution of the higher excitations to the rotationally summed inelastic ICS.

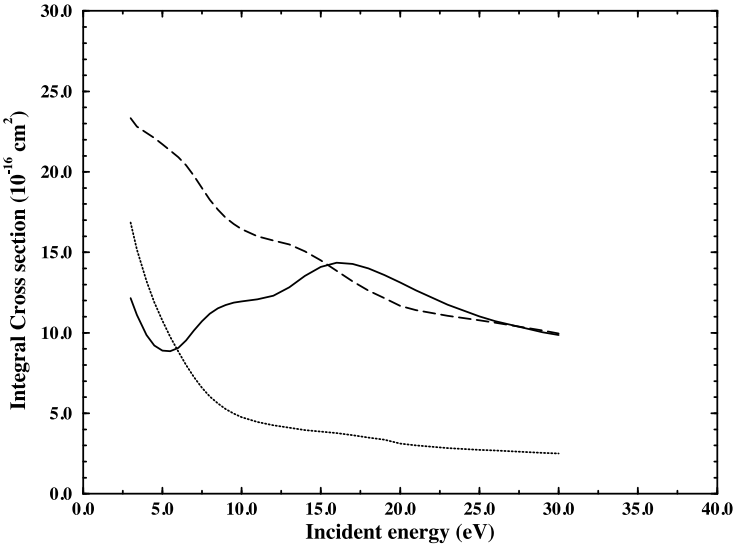

Figure 9. Rotational excitation ICS. Solid line: rotationally elastic; long–dashed curve: inelastic rotationally summed; dotted curve: dipole-allowed ($J = 0 \rightarrow J' = 1$) excitation.

5. Conclusions

The combination of SMCPP, FBA and ANR approximations has provided an efficient tool to study elastic and rotationally inelastic electron scattering by SO_2 molecules. Our integral and momentum transfer elastic (rotationally summed) cross sections are in good agreement with available experimental data, especially at lower incident energies ($E < 15$ eV). A very good agreement with experiment is also found in the differential elastic cross sections, even at low energies such as 3.4 and 5 eV. Since we have performed static-exchange calculations, this fact indicates that the long-range dipole interactions may be more relevant in the description of the scattering process than polarization effects. Our elastic DCSs also agree well with the results of Gil and Rescigno [12] and of Gianturco *et al* [11], but there were some discrepancies between our results for ICS, MTCS and rotational excitations and the theoretical results of [11] (figures 5–8).

We have also found that rotationally inelastic cross sections for e^-–SO_2 collisions are very large, exceeding the rotationally elastic cross sections at lower energies ($E < 15$ eV). Although the dipole-allowed ($J = 0 \rightarrow J' = 1$) rotational excitation is always relevant, it was found that higher rotational excitations also give significant contributions to the rotationally summed inelastic ICS.

Acknowledgments

The authors acknowledge partial support from Brazilian agency Conselho Nacional de Desenvolvimento Científico e Tecnológico (CNPq). APPN and MTdNV acknowledge support from Fundação de Amparo à Pesquisa do Estado de São Paulo (FAPESP). MHFB acknowledges partial support from Fundação da Universidade Federal do Paraná para o Desenvolvimento da Ciência, da Tecnologia e da Cultura (FUNPAR). Our calculations were made at CENAPAD-SP, CENAPAD-NE and CCE-UFPR.

References

[1] Ferm M and Svanberg P-A 1998 *Atmos. Environ.* **32** 1377
[2] Smyth W H and Marconi M L 1998 *J. Geophys. Res.* **103** 9083
[3] van der Burgt P J M, Antaya M E and McConkey J W 1992 *Z. Phys.* D **24** 125
[4] Orient O J and Srivastava S K 1984 *J. Chem. Phys.* **80** 140
Čadež I M, Pejčev V M and Kurepa M V 1983 *J. Phys. D: Appl. Phys.* **16** 305
Smith O I and Stevenson J S 1981 *J. Chem. Phys.* **74** 6777
[5] Andrić L, Čadež I, Hall R I and Zubek M 1983 *J. Phys. B: At. Mol. Phys.* **16** 1837
[6] Szmytkowski C and Maciag K 1986 *Chem. Phys. Lett.* **124** 463
Sokolov V F and Sokolova Y A 1981 *Sov. Tech. Phys. Lett.* **7** 268
[7] Gulley R J and Buckman S J 1994 *J. Phys. B: At. Mol. Opt. Phys.* **27** 1833
[8] Trajmar S and Shyn T W 1989 *J. Phys. B: At. Mol. Opt. Phys.* **22** 2911
[9] Ali M A, Kim Y-K, Hwang W and Rudd M E 1998 *J. Korean Phys. Soc.* **32** 499
[10] Hayashi M 1987 *Swarm Studies and Inelastic Electron–Molecule Collisions* ed L C Pitchford *et al* (Springer: New York) p 167
[11] Gianturco F A, Paioletti P and Sanna N 1997 *J. Phys. B: At. Mol. Opt. Phys.* **30** 4535
[12] Gil T and Rescigno T N 1993 Private communication
[13] Takatsuka K and McKoy V 1981 *Phys. Rev.* A **24** 2473
Takatsuka K and McKoy V 1984 *Phys. Rev.* A **30** 1734
[14] Bettega M H F, Ferreira L G and Lima M A P 1993 *Phys. Rev.* A **47** 1111
[15] Bachelet G B, Hamann D R and Schlüter M 1982 *Phys. Rev.* B **26** 4199
[16] Varella M T do N, Bettega M H F, Lima M A P and Ferreira L G 1999a *J. Chem. Phys.* **11** 6369
Natalense A P P, Bettega M H F, Ferreira L G and Lima M A P 1999b *Phys. Rev.* A **59** 879
Varella M T do N, Ferreira L G and Lima M A P 1999c *J. Phys. B: At. Mol. Opt. Phys.* **32** 2031
Bettega M H F, Varella M T do N, Ferreira L G and Lima M A P 1998a *J. Phys. B: At. Mol. Opt. Phys.* **31** 4419
Bettega M H F, Lima M A P and Ferreira L G 1998b *J. Phys. B: At. Mol. Opt. Phys.* **31** 2091
Bettega M H F, Oliveira A J S, Natalense A P P, Lima M A P and Ferreira L G 1998c *Eur. Phys. J.* D **1** 291
[17] Bettega M H F, Ferreira L G and Lima M A P 1998 *Phys. Rev.* A **57** 4987
Natalense A P P, Sartori C S, Ferreira L G and Lima M A P 1996 *Phys. Rev.* A **54** 5435
[18] Varella M T do N, Natalense, A P P, Bettega, M H F and Lima M A P 1999 *Phys. Rev.* A **60** 3684
[19] Varella M T do N, Bettega M H F, da Silva A J R and Lima M A P 1999 *J. Chem. Phys.* **110** 2452
[20] Varella M T do N, Bettega M H F and Lima M A P 1997 *Z. Phys.* D **39** 59
[21] Natalense A P P, Ferreira L G and Lima M A P 1998 *Phys. Rev. Lett.* **81** 3832
[22] Chase D M 1956 *Phys. Rev.* **104** 838
[23] Temkin A and Vasavada K V 1967 *Phys. Rev.* **160** 109
[24] Gianturco F A and Jain A 1986 *Phys. Rep.* **143** 347
[25] Lide D R 1997–8 *CRC Handbook of Chemistry and Physics* 78th edn (Boca Raton, FL: Chemical Rubber Company) p 9–45
[26] Norcross D W and Collins L A 1982 *Adv. Atom. Mol. Phys.* **18** 341
[27] Yuan J and Zhang Z 1992 *Phys. Rev.* A **45** 4565
[28] Isaacs W A and Morrison M A 1996 *Phys. Rev.* A **53** 4215
[29] Gianturco F A, Mukherjee T and Paioletti P 1997 *Phys. Rev.* A **56** 3638
[30] Lima M A P and McKoy V 1988 *Phys. Rev.* A **38** 501
Lima M A P and McKoy V 1990 *Phys. Rev.* A **41** 327
[31] Rose M E 1957 *Elementary Theory of Angular Momentum* (New York: Wiley)
[32] Van Winter C 1954 *Physica* **20** 274
[33] Jain A and Thompson D G 1983 *Comput. Phys. Commun.* **30** 301
[34] Altshuler S 1957 *Phys. Rev.* **107** 114
[35] Bettega M H F, Natalense A P P, Lima M A P and Ferreira L G 1996 *Int. J. Quantum Chem.* **60** 821
[36] Hehre W J, Radon L, Schleyer P v R and Pople J A 1986 *Ab Initio Molecular Orbital Theory* (New York: Wiley) p 182
[37] Lide D R 1997–8 *CRC Handbook of Chemistry and Physics* 78th edn (Boca Raton, FL: Chemical Rubber Company) pp 10–204